Hydraulic response of fibre-reinforced sand subject to seepage

K.-H. Yang[1], W. M. Adilehou[2], S.-T. Jian[3] and S.-B. Wei[4]

[1]Associate Professor, Department of Civil Engineering, National Taiwan University (NTU), 1, Sec. 4, Roosevelt Rd., Taipei 106, Taiwan, E-mail: khyang@ntu.edu.tw (corresponding author)
[2]PhD Candidate, Department of Civil and Construction Engineering, National Taiwan University of Science and Technology (Taiwan Tech), 43, Sec. 4, Keelung Rd., Taipei 106, Taiwan, E-mail: willmathfr83@gmail.com
[3]Graduate Student, Department of Civil and Construction Engineering, National Taiwan University of Science and Technology (Taiwan Tech), 43, Sec. 4, Keelung Rd., Taipei 106, Taiwan, E-mail: kalankyo@gmail.com
[4]Graduate Student, Department of Civil and Construction Engineering, National Taiwan University of Science and Technology (Taiwan Tech), 43, Sec. 4, Keelung Rd., Taipei 106, Taiwan, E-mail: freemopa@gmail.com

Received 09 January 2017, revised 11 April 2017, accepted 19 May 2017

ABSTRACT: A series of upward seepage tests on unreinforced and reinforced sand specimens was conducted to investigate the influence of soil density and fibre parameters (i.e. fibre contents and lengths) on the piping failure mode, hydraulic conductivity k, and critical hydraulic gradient i_{cr} of fibre-reinforced soil (FRS). Direct shear tests were also performed to establish the relationships between soil shear strength and i_{cr} of FRS. A dataset of seepage tests on FRS was compiled from a literature review to assess the overall variation of k and i_{cr} with fibre content. The test results revealed that k decreases and i_{cr} increases as the fibre content increases. The fibre is more effective in dense specimens than in loose specimens. The test results also indicate the i_{cr} of FRS is strongly correlated to its soil shear strength. Finally, two case examples, unreinforced and reinforced embankments subject to flood-induced elevated water level, were analysed numerically. The numerical results demonstrated that the embankment backfilled with FRS possessed the combined merits of soil improvement in both mechanical and hydraulic performance. The use of FRS as backfill can effectively delay the advance of seepage, reduce soil piping potential, and improve system slope stability against seepage.

KEYWORDS: Geosynthetics, Fibre-reinforced sand, Critical hydraulic gradient, Hydraulic conductivity, Flood

REFERENCE: Yang, K.-H., Adilehou, W. M., Jian, S.-T. and Wei, S.-B. (2017). Hydraulic response of fibre-reinforced sand subject to seepage. *Geosynthetics International*. [http://dx.doi.org/10.1680/jgein.17.00017]

1. INTRODUCTION

Hydraulic failures of geotechnical earth structures are caused by impacts from wave forces, toe scour, overtopping, and soil piping and erosion (Brandl 2011). As taller hydraulic structures are constructed because of rising flood levels due to the influence of global warming and extreme weather, the increasing hazards of soil piping and erosion have gained much attention (Rice *et al*. 2007; Rice and Duncan 2010; Polemio and Lollino 2011; Danka and Zhang 2015).

Past case studies have reported that failures of many man made earth fill structures, natural soil masses, and rock deposits (e.g. landslide dams) have been associated with seepage-induced piping and erosion (Hagerty 1991a, 1991b; Foster *et al*. 2000; Fell *et al*. 2003; Xu and Zhang 2009; Zhang *et al*. 2009; Garner and Fannin 2010; Peng and Zhang 2012). Danka and Zhang (2015) reported that the failure rate of dikes, man-made dams, and landslide dams caused by piping are 14%, 37%, and 8%, respectively. Richards and Reddy (2007) reported that approximately half of the world's dams have experienced soil erosion. Consequently, mitigating seepage-induced adverse impacts and enhancing the stability of the earth structures has become an urgent and challenging issue in waterfront protection.

Effective countermeasures against soil piping involve the use of cut-off walls, impervious blankets, and pressure relief wells to reduce the hydraulic gradient within the soil, or the use of soil improvement and filter layers to increase soil piping resistance. Among these measures, soil improvement through fibre reinforcement is

the focus of this study. Fibre reinforcement is a technique whereby randomly distributed natural or synthetic fibres are mixed uniformly with soil to improve its mechanical and hydraulic performance in geotechnical and geoenvironmental applications. Essentially, random discrete flexible fibres provide reinforcement functions, approximating the natural behaviour of plant roots holding the soil. Fibre reinforcement has proven to be a promising technique for projects involving stabilising thin soil veneers, repairing locally failed slopes, improving the bearing capacity of soft ground, strengthening soil in footings, pavement, and earth retaining walls, enhancing soil piping resistance in hydraulic structures, increasing dynamic resistance to liquefaction, reducing surficial soil erosion, and mitigating desiccation cracking of compacted clay systems (Santoni *et al*. 2001; Zornberg 2002; Jamshidi *et al*. 2010; Liu *et al*. 2011; Hejazi *et al*. 2012; Collins *et al*. 2015; Pino and Baudet 2015).

The majority of previous studies have focused on the mechanical behaviour of fibre-reinforced soil (FRS), and demonstrated that mixing fibre with soil can effectively enhance peak shear strength and reduce the loss of post-peak shear strength (Gray and Ohashi 1983; Gray and Al-Refeai 1986; Maher and Gray 1990; Ranjan *et al*. 1994; Michalowski and Zhao 1996; Consoli *et al*. 2002, 2005 2007, 2009a 2009b; Zornberg 2002; Michalowski and Čermák 2003; Yetimoglu and Salbas 2003; Yilmaz 2009; Ahmad *et al*. 2010; Diambra *et al*. 2010; Marin *et al*. 2010; Sadek *et al*. 2010; Li and Zornberg 2013; Li *et al*. 2014; Shao *et al*. 2014; Anggraini *et al*. 2015). Soil type, fibre type, length, and content, as well as cement content and compaction conditions, are the key parameters evaluated in these studies (Najjar *et al*. 2013; Chou *et al*. 2016).

In contrast to the studies on mechanical behaviour of FRS, studies on the hydraulic performance of FRS are relatively limited. Only a few studies of experimental seepage tests on FRS (Furumoto *et al*. 2002; Sivakumar Babu and Vasudevan 2008; Das *et al*. 2009; Das and Viswanadham 2010; Estabragh *et al*. 2014, 2016; De Camillis *et al*. 2016) and model tests for levees reinforced with short fibres (Furumoto *et al*. 2002) have been reported in the literature. In summary, these studies have found that fibre reinforcement can effectively enhance the piping resistance of soil by deferring the occurrence of soil piping at a high hydraulic gradient. The aforementioned studies primarily focused on the effect of fibre parameters (i.e. fibre type, length, and content) on the hydraulic gradient and the associated piping resistance of FRS. Little attention has focused on the effect of fibre parameters on the hydraulic conductivity of FRS, which is another crucial hydraulic parameter of FSR. Furthermore, the overall performance of hydraulic structures backfilled with FRS has not been fully investigated. Further investigation on the combined merits of soil improvement by fibre in both mechanical and hydraulic performance (i.e. increasing soil shear strength and piping resistance) is necessary.

The preceding discussion is the basis of this study, which involved conducting a series of upward seepage tests on unreinforced and reinforced sands. The objectives of this study are as follows: (1) to evaluate the influence of soil density and fibre parameters (i.e. fibre length and content) on the hydraulic responses (i.e. piping failure mode, hydraulic conductivity, and critical hydraulic gradient) of FRS; (2) to establish the relationship between the critical hydraulic gradient and the shear strength parameter of FRS; and (3) to perform numerical analyses of unreinforced and reinforced embankments subject to flooding to evaluate the combined effects of fibre inclusion on improving the mechanical and hydraulic performance of soil. In addition, a dataset of seepage tests on FRS was compiled from the literature. The overall variation of hydraulic conductivity and critical hydraulic gradient of FRS with fibre content was assessed and discussed. The results and discussion in this study provide insightful information for the application of FRS to hydraulic structures.

2. EXPERIMENTAL PROGRAMME

2.1. Test system

A series of seepage tests was conducted to evaluate the influences of soil density and fibre parameters on the hydraulic conductivity and critical hydraulic gradient of FRS. For this purpose, an upward seepage test system (Figure 1), consisting of a constant head device, a permeameter, and measuring systems, was developed in this study and is described in this section.

The constant head device contains an elevated water supply reservoir and a water barrel positioned at a lower elevation. The water reservoir was connected to the permeameter by a pipe 1.5 cm in diameter that provided a steady flow of water to the soil specimen. To maintain a constant head, an overflow device with a free discharge board was constructed inside the water supply reservoir (Figure 1). A pump with a maximum capacity of 40 l/min was placed inside the barrel to redirect water back to the water supply reservoir. The overflow device and pump enabled the water to move in a closed loop, creating an automatic water recycling system. The elevation of the water reservoir could be adjusted using a pulley device; positioning the water reservoir at various heights yielded different values for the hydraulic head during testing.

The permeameter consists of a cylindrical cell (10.5 cm in diameter and 38 cm in height) and a bottom pedestal. The cylindrical cell was composed of transparent acrylic, enabling visual observations of seepage and piping progress in soil specimens during tests. To avoid a scale effect, the ratio of the specimen diameter to the mean grain diameter of sand in this test was 90, which is larger than the values (8–12) specified in ASTM (ASTM D2434). Additionally, the diameter of the specimen (i.e. 10.5 cm) also satisfies the ASTM requirement (i.e. cylinder diameter >7.6 cm) with respect to the grain sizes of the used soils. The pedestal, filled with marbles and covered with porous screens, was used to distribute the upward seepage evenly across the soil specimen. The marbles were used to minimise the high-pressure water jet

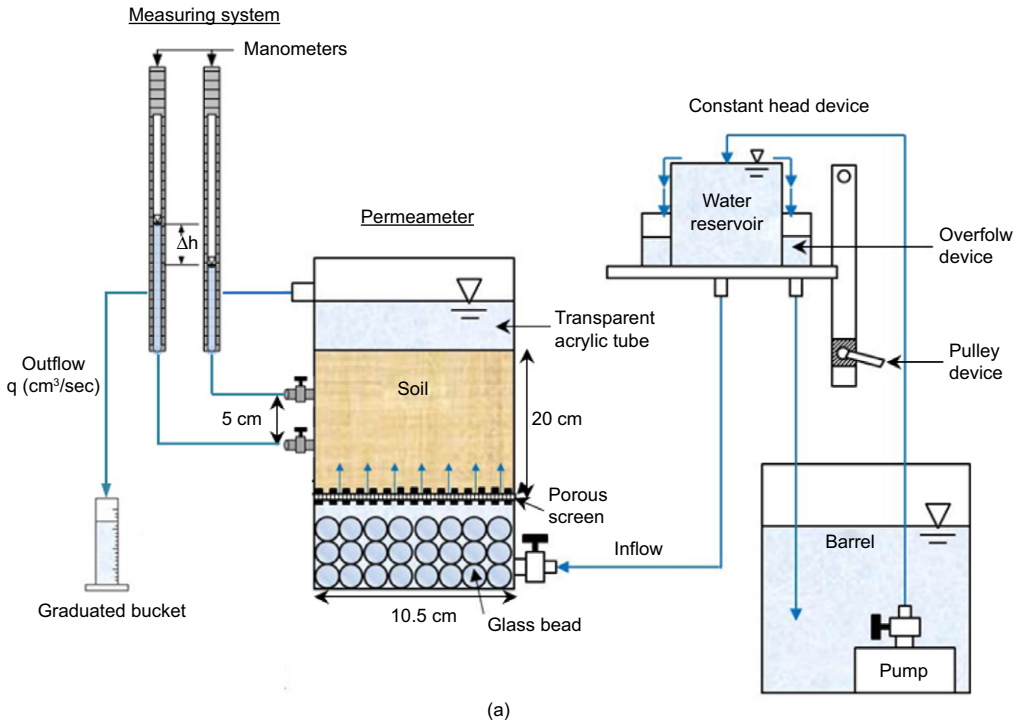

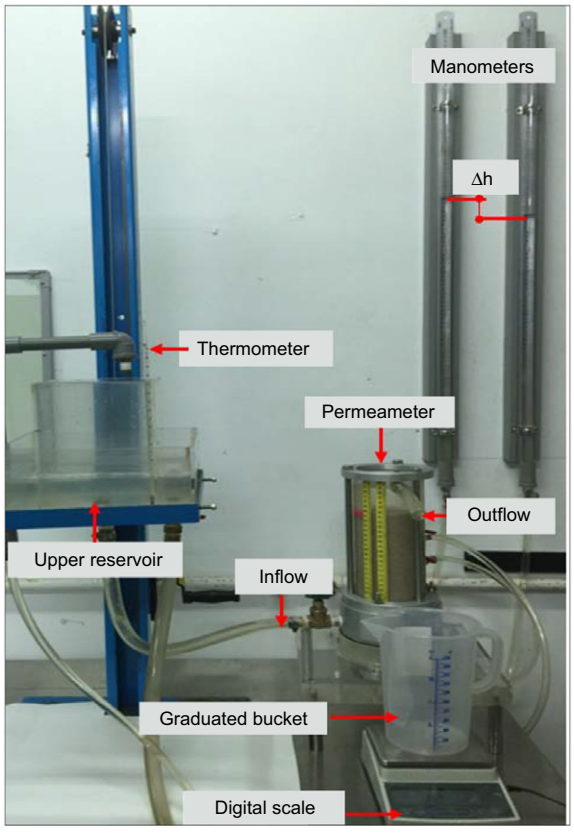

Figure 1. Upward seepage test system: (a) schematic illustration; (b) overview photo

effect from the elevated water reservoir. The porous screens comprised two perforated metal plates and a nonwoven geotextile. The perforated metal plates, with numerous punched holes, were used to support the overburden pressure from soil specimens. The nonwoven geotextile was placed between the two perforated metal plates and served as a filter to prevent the loss of soil. The nonwoven geotextile was carefully selected so that its hydraulic conductivity was much greater than that of the test soil.

The water flow from the top of the specimen was measured and then discharged to the barrel. Discharge velocity v at a given hydraulic gradient was calculated by dividing the collected volume of discharge at a certain time period by the cross-sectional area of the soil specimen. The permeameter cylinder was perforated at distances of 7 and 12 cm from the bottom of the specimen (Figure 1) and connected to graduated manometers to measure hydraulic head difference (i.e. head loss) at a given distance of the seepage path. The corresponding hydraulic gradient i can then be calculated at each stage of the test using the following equation:

$$i = \frac{\Delta h}{L} \quad (1)$$

where Δh is the head difference between two manometers and L (=5 cm) is the distance between the two measuring valves connected to the manometers.

2.2. Test material and test programme

Uniform quartz sand was tested in this study. Figure 2 presents the grain size distribution curve of the test soil. Table 1 summarises the soil properties. The test soil has a mean particle size d_{50} value of 1.12 mm and is classified as poorly graded sand (SP) according to the Unified Soil Classification System (USCS). The specific gravity, G_s, the coefficient of uniformity, C_u, and curvature, C_c, were 2.65, 2.02, and 1.08, respectively. The minimum and maximum dry unit weights of sand, conducted in accordance with ASTM D4254 and D4253, were $\gamma_{d,min} = 13.92$ kN/m^3 and $\gamma_{d,max} = 15.35$ kN/m^3. The sand was carefully prepared at two target relative densities ($D_r = 50\%$ and 70%) to represent loose and dense soil conditions. Based on the constant head test results presented later, the saturated hydraulic conductivity of the soil was $k = 8.2 \times 10^{-3}$ and 6.1×10^{-3} m/s, and the critical hydraulic gradient of the soil was $i_{cr} = 0.86$ and 0.92 for soil at $D_r = 50\%$ and 70%, respectively.

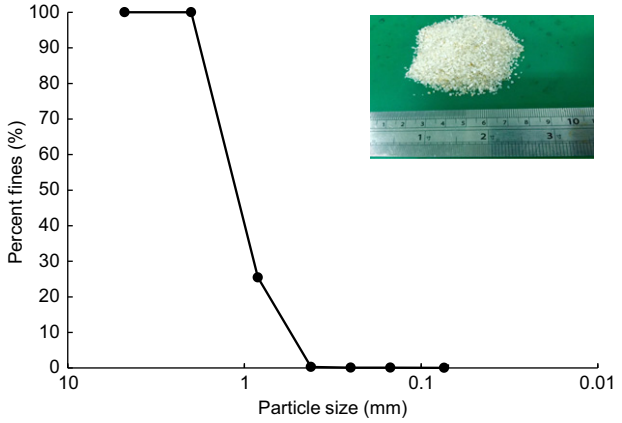

Figure 2. Grain size distribution curve and photo of the test sand

Table 1. Summary of test soil properties

Soil properties	Value
Specific gravity G_s	2.65
Effective particle size d_{10} (mm)	0.61
Mean particle size d_{50} (mm)	1.12
Uniformity coefficient C_u	2.02
Coefficient of curvature C_c	1.08
Soil classification (USCS)	SP
Maximum dry unit weight $\gamma_{d,max}$ (kN/m^3)	15.35
Minimum dry unit weight $\gamma_{d,min}$ (kN/m^3)	13.92
Maximum void ratio e_{max}	0.87
Minimum void ratio e_{min}	0.63
[a]Hydraulic conductivity of soil k (m/s)	8.2×10^{-3} and 6.1×10^{-3}
[a]Critical hydraulic gradient of soil i_{cr}	0.86 and 0.92

[a]Values are for soil density $D_r = 50\%$ and 70%, respectively.

Polypropylene (PP) fibre was used in this study. PP fibre is the most widely adopted synthetic fibre for soil reinforcement (Yetimoglu *et al.* 2005; Khattak and Alrashidi 2006). Das and Viswanadham (2010) reported that PP fibre performed better than polyester (PET) fibre in increasing seepage resistance, because the PET fibre has a specific gravity higher than the PP fibre. For the same fibre content, a greater specific gravity implies a lower fibre volume and a lower number of fibres, and hence reduces the benefit of improving the piping resistance of a soil. The PP fibre tested in this study has a circular cross-section with an average diameter of 0.0577 mm. The specific gravity of the fibre is $G_{sf} = 0.91$, slightly lower than that of water. Table 2 summarises the physical and mechanical properties of the test fibre.

A total of 20 seepage tests were conducted on both unreinforced and reinforced soil specimens. The test variables are soil relative density ($D_r = 50\%$ and 70%), fibre content ($\omega_f = 0\%$, 0.5%, 1.0%, and 1.5%), and fibre length ($L_f = 6$, 12, and 19 mm). Table 3 lists the seepage test program. The test numbering was defined as follows. The first part, a letter 'R' or 'U,' indicates a reinforced or unreinforced specimen, respectively. The second, third, and fourth parts denote soil relative density, fibre content, and fibre length, respectively. For example, U-50 indicates an unreinforced specimen with soil relative density $D_r = 50\%$ and R-70-0.5-6 indicates a reinforced specimen with soil relative density $D_r = 70\%$, fibre content $\omega_f = 0.5\%$ and fibre length $L_f = 6$ mm.

2.3. Specimen preparation and test procedure

The specimens were prepared at loose and dense conditions (i.e. Test Series L and D), corresponding to soil

Table 2. Physical and mechanical properties of fibre

Properties	Value
Type	Polypropylene (PP) fibre
Cross-section shape	Circular
Equivalent diameter d_f (mm)	0.0557
Length L_f (mm)	6, 12, 19
Specific gravity G_{sf}	0.91
Denier (g/9000 m)	20
Ultimate tensile strength (MPa)	250
Melting point (°C)	160~170
Water absorption	No

Table 3. Summary of seepage test conditions and results

Test	ω_f (%)	L_f (mm)	i_{cr}	i_{cr} ratio	k (m/s)	k ratio
Test series L (loose specimen)						
U-50	0.0	0	0.86	1.00	8.2×10^{-3}	1.00
R-50-0.5-6	0.5	6	1.16	1.35	4.3×10^{-3}	0.52
R-50-1-6	1.0	6	1.20	1.40	3.7×10^{-3}	0.45
R-50-1.5-6	1.5	6	1.52	1.77	2.2×10^{-3}	0.27
R-50-0.5-12	0.5	12	1.08	1.26	5.3×10^{-3}	0.65
R-50-1-12	1.0	12	1.30	1.51	4.4×10^{-3}	0.54
R-50-1.5-12	1.5	12	1.52	1.77	3.2×10^{-3}	0.39
R-50-0.5-19	0.5	19	1.14	1.33	6.5×10^{-3}	0.79
R-50-1-19	1.0	19	1.34	1.56	3.9×10^{-3}	0.48
R-50-1.5-19	1.5	19	1.36	1.58	3.5×10^{-3}	0.43
Test series D (dense specimen)						
U-70	0.0	0	0.92	1.00	6.1×10^{-3}	1.00
R-70-0.5-6	0.5	6	1.28	1.39	4.1×10^{-3}	0.68
R-70-1-6	1.0	6	1.40	1.52	2.8×10^{-3}	0.46
R-70-1.5-6	1.5	6	1.94	2.11	1.4×10^{-3}	0.24
R-70-0.5-12	0.5	12	1.22	1.33	3.3×10^{-3}	0.54
R-70-1-12	1.0	12	1.50	1.63	3.1×10^{-3}	0.51
R-70-1.5-12	1.5	12	1.74	1.89	2.5×10^{-3}	0.41
R-70-0.5-19	0.5	19	1.28	1.39	4.1×10^{-3}	0.67
R-70-1-19	1.0	19	1.36	1.48	3.3×10^{-3}	0.54
R-70-1.5-19	1.5	19	1.62	1.76	2.5×10^{-3}	0.41

relative density $D_r = 50\%$ and 70%, respectively. Each specimen was carefully prepared to ensure that its soil had a uniform density and full saturation. The required weight of dry soil for the target relative density was determined using the relative density equation:

$$D_r = \frac{e_{max} - e}{e_{max} - e_{min}} \quad (2)$$

where e_{max}, e_{min}, and e are the maximum, minimum, and target void ratios of soil. The desired weight of fibre for reinforced specimens was determined considering the dry weight of the soil and the desired gravimetric fibre content, as expressed in Equation (3):

$$\omega_f = \frac{W_f}{W_s} \quad (3)$$

where W_f and W_s are the dry weight of fibre and soil, respectively.

A known quantity of soil and fibre was carefully mixed by hand. The hand mixing method has been commonly adopted by various researchers (Ranjan *et al.* 1994; Consoli *et al.* 2002, 2007; Yetimoglu and Salbas 2003; Yetimoglu *et al.* 2005; Das *et al.* 2009; Estabragh *et al.* 2014). The soil–fibre mixture was moisturised by adding water (10% of total weight) to avoid soil–fibre segregation before being spread into the permeameter. The permeameter was carefully filled with the wet soil–fibre mixture in five layers (4 cm thick for each layer). Each layer was compacted using a metal rod to control its height. This procedure was repeated until the desired specimen height ($H = 20$ cm) was reached. Visual inspection showed that good uniformity was achieved. The repeatability and consistency of the test results were verified by examining test results performed under the same conditions. Figure 3 shows two demonstration examples of test repeatability.

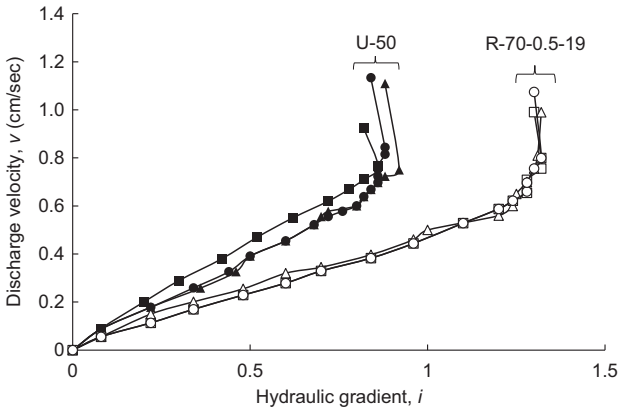

Figure 3. Demonstration examples of test repeatability

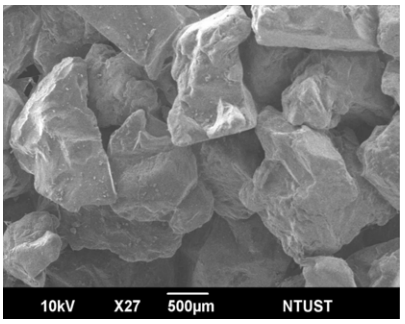

(a)

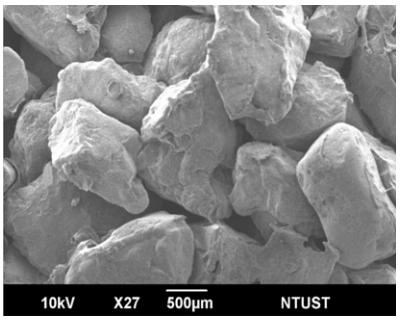

(b)

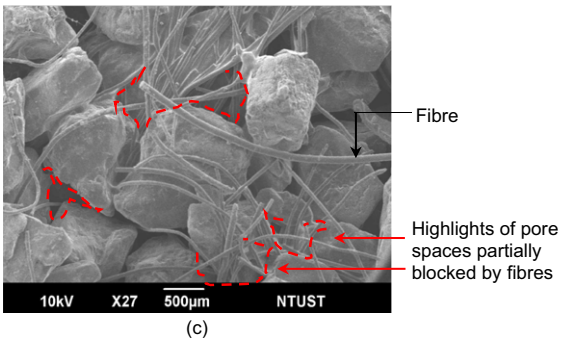

(c)

Figure 4. Scanning electron microscope (SEM) photo: (a) unreinforced sand at $D_r = 50\%$ (U-50); (b) unreinforced sand at $D_r = 70\%$ (U-70); (c) fibre-reinforced sand (R-70-1-6)

Figure 4 shows the scanning electron microscope (SEM) photographs of unreinforced specimens at different relative densities (Figures 4a and 4b) and the FRS

specimen of R-70-1-6 (Figure 4c). The interaction between fibres and soil grains can be clearly observed from Figure 4c. Compared with unreinforced sand, some soil pore spaces (as highlighted by red dashed lines in Figure 4c) of the reinforced sand were partially filled by the fibres. Consequently, the fibres could block some pore channels for seepage and restrict the seepage flow within these pore channels.

After specimen preparation, the specimen was submerged in water and subjected to a constant seepage flow under a low hydraulic head that did not affect the specimen stability for 24 h to ensure the full saturation of specimens. Afterward, the seepage test began by applying a series of incrementally increased hydraulic heads to the specimen until soil piping failure occurred. The applied hydraulic head was increased by 2 cm (approximately $\Delta i = 0.1$) for each increment and maintained for at least 10 min until the hydraulic heads in the manometers stabilised, indicating that equilibrium was reached. The hydraulic gradient i and corresponding discharge velocity v were recorded in each stage of the test.

3. RESULTS AND DISCUSSION

In this section, the test results including seepage failure mode and the i–v relations were analysed and discussed. The i–v plots were used to determine the k and i_{cr} of FRS. The influence of soil density and fibre parameters on the hydraulic responses of FRS is quantitatively evaluated and discussed, and the relationship between the critical hydraulic gradient and the shear strength of FRS is established.

3.1. Failure mode

Figure 5 shows the typical failure modes of unreinforced and reinforced specimens at and after the critical hydraulic gradient i_{cr}. For the unreinforced specimen at i_{cr} (Figure 5a), the specimen (U-70) exhibited an expansion (≈0.8 cm). At this stage, the soil seemed to have liquefied (the author's finger could easily penetrate into the specimen without feeling much resistance). When the next hydraulic head increment after i_{cr} was applied, the specimen showed a sudden and notable heave (≈2 cm), followed by the sand piping/boiling phenomenon

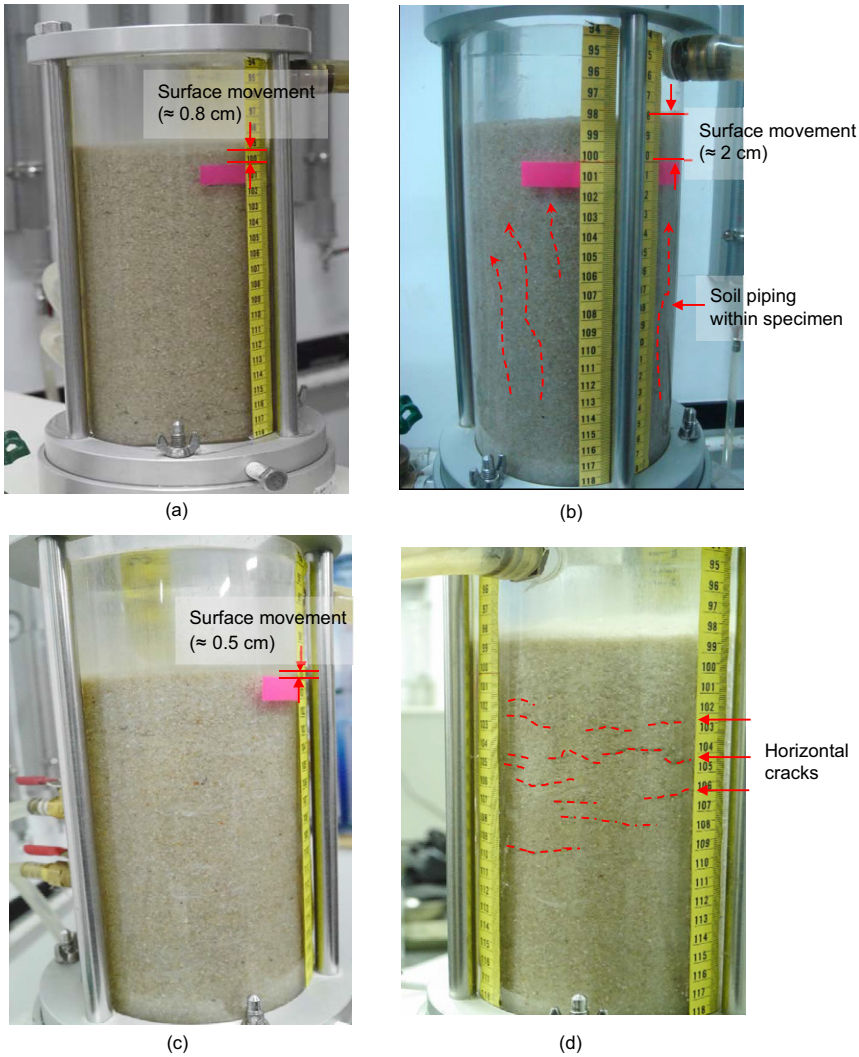

Figure 5. Failure mode of unreinforced and reinforced specimens: (a) U-70 at $i_{cr} = 0.92$; (b) U-70 at the next applied hydraulic head increment after i_{cr}; (c) R-70-1.5-19 at $i_{cr} = 1.62$; (d) development of horizontal cracks of R-70-1.5-19 at the next applied hydraulic head increment after i_{cr}

(Figure 5b). The soil lost its overall stability. The heave and boiling phenomenon are strong evidence of soil failure subjected to seepage. The soil boiling happened globally within the unreinforced specimen in which soil particles were forced to migrate with the upward seepage. Vigorous soil boiling on top of the specimen can also be clearly observed.

For the reinforced specimen at i_{cr} (Figure 5c), the specimen (R-70-1.5-19) displayed an isotropic failure mode: soil experienced a uniformly slight heave (≈0.5 cm). At this stage (onset of soil seepage failure), the surface movement of the reinforced specimen is smaller than that of the unreinforced specimen even though the reinforced specimen was subject to a seepage force ($i_{cr} = 1.62$) higher than that of the unreinforced specimen ($i_{cr} = 0.92$). Figure 5d shows the failure mode of the reinforced specimen when the next hydraulic head increment after i_{cr} was applied. Several horizontal micro-cracks developed within the specimen at this stage. It is also observed that the development of horizontal cracks concentrated at the middle and top of the specimen. Fewer cracks at the bottom of the specimen are likely due to the influence of higher overburden pressure at the bottom, which prevents the soil from failure in tension.

The development of horizontal cracks within the reinforced specimen indicates significant distress on the specimen upon seepage force. The observed horizontal cracks also reveal that the seepage force induced tensile force could have exceeded the tensile resistance provided by fibres in local areas within the specimen; consequently, soil particles in these areas tend to separate and then the cracks develop. The horizontal cracks could enlarge with an increase in the applied hydraulic head. Unlike the failure mode of the unreinforced specimen, the reinforced specimen experienced neither global soil piping within the specimen nor vigorous soil boiling on top of the specimen. This observation demonstrates that fibre can effectively bind soil together against seepage and convert the vigorous soil erosion and piping in the unreinforced soil to a global and isotropic soil expansion.

3.2. *i–v* Relations

Figures 6 and 7 show the *i–v* plots for different soil densities, fibre contents, and fibre lengths. The *i–v* curves consist of two parts. In the first part of the curves, the *v* value increases linearly with *i*. The flow is laminar and the hydraulic conductivity *k* can be obtained according to Darcy's law (i.e. $v = ki$). In the second part of the curves, the *i–v* curves exhibit either a drastic increase in the discharge velocity or a decrease in the measured hydraulic gradient. Both phenomena indicate a change in the hydraulic behaviour of specimens, suggesting the occurrence of the soil seepage failure. The critical hydraulic gradient was determined at one stage prior to this stage. Table 3 summarises the test results of *k* and i_{cr}.

Although the system total head was increased by elevating the upper water reservoir, the drop in the hydraulic gradient after i_{cr} suggests the relief of accumulated porewater pressure within specimens after soil piping failure (Figure 5a) and the development of horizontal cracks (Figure 5d). The drop can also be explained by the fact that the head loss of seepage through specimens decreased because of the loosened soil packing state after the soil seepage failure. A pressure drop has also been observed in experimental and field tests (Nichols *et al*. 1994; Parekh *et al*. 2016). Consequently, the water pressure measured at this stage cannot represent the real hydraulic conditions, specifically for hydraulic gradient, across the specimen.

Figures 6 and 7 clearly reveal that for specimens at the same relative density and fibre length, the *i–v* curves shift to the right as the fibre content increases, signifying an increase in i_{cr} and a decrease in *k*. The experimental results are likely to result from the fibre inclusion providing tensile resistance against soil piping and erosion, and restricting the seepage flow within some pore channels that were partially blocked by fibres. An increase in the critical hydraulic gradient of FRS with fibre content was also reported in Das *et al*. (2009), Das and Viswanadham (2010), Estabragh *et al*. (2014, 2016), and Sivakumar Babu and Vasudevan (2008). A detailed and quantitative evaluation of the effect of fibre content and length follows in the next section.

3.3. Effect of fibre parameters

This section discusses the effect of fibre parameters (i.e. fibre content and length) on the hydraulic response of FRS. The variation of *k* and i_{cr} with fibre parameters was quantitatively evaluated using the *k* and i_{cr} ratios, defined as the ratios of the hydraulic conductivity and critical hydraulic gradient of FRS to those of unreinforced sand. The *k* and i_{cr} ratios serve as indices for assessing the reduction of seepage velocity and improvement of soil piping resistance.

Figure 8 shows the influence of fibre content on *k* and i_{cr}, and Table 3 lists the associated *k* and i_{cr} ratio values. A clear trend of increasing i_{cr} and decreasing *k* with increasing fibre content can be observed, regardless of soil density. For example, for FRS with $L_f = 6$ mm in Test Series L, the *k* decreases from 8.2×10^{-3} to 2.2×10^{-3} m/s (*k* ratio decreases from 1.0 to 0.27) and the i_{cr} increases from 0.86 to 1.52 (i_{cr} ratio increases from 1.0 to 1.77) as the fibre content increases from 0 to 1.5%. These results suggest that soil piping resistance increases to 177%, and hydraulic conductivity decreases to 27% of that of unreinforced sand after adding 1.5% of fibre to the soil. Similarly, for FRS with $L_f = 6$ mm in Test Series D, the *k* decreases from 6.1×10^{-3} to 1.4×10^{-3} m/s (*k* ratio decreases from 1.0 to 0.24) and the i_{cr} increases from 0.92 to 1.94 (i_{cr} ratio increases from 1.0 to 2.11) as the fibre content increases from 0 to 1.5%.

The test results also reveal that the fibre has a greater effect in dense specimens (Test Series D) than in loose specimens (Test Series L); at a given fibre length and content, the larger i_{cr} and smaller *k* values were measured for dense specimens. The high i_{cr} improvement likely results from increased soil–fibre interaction in dense soil states, and the high *k* reduction is attributable to the fact

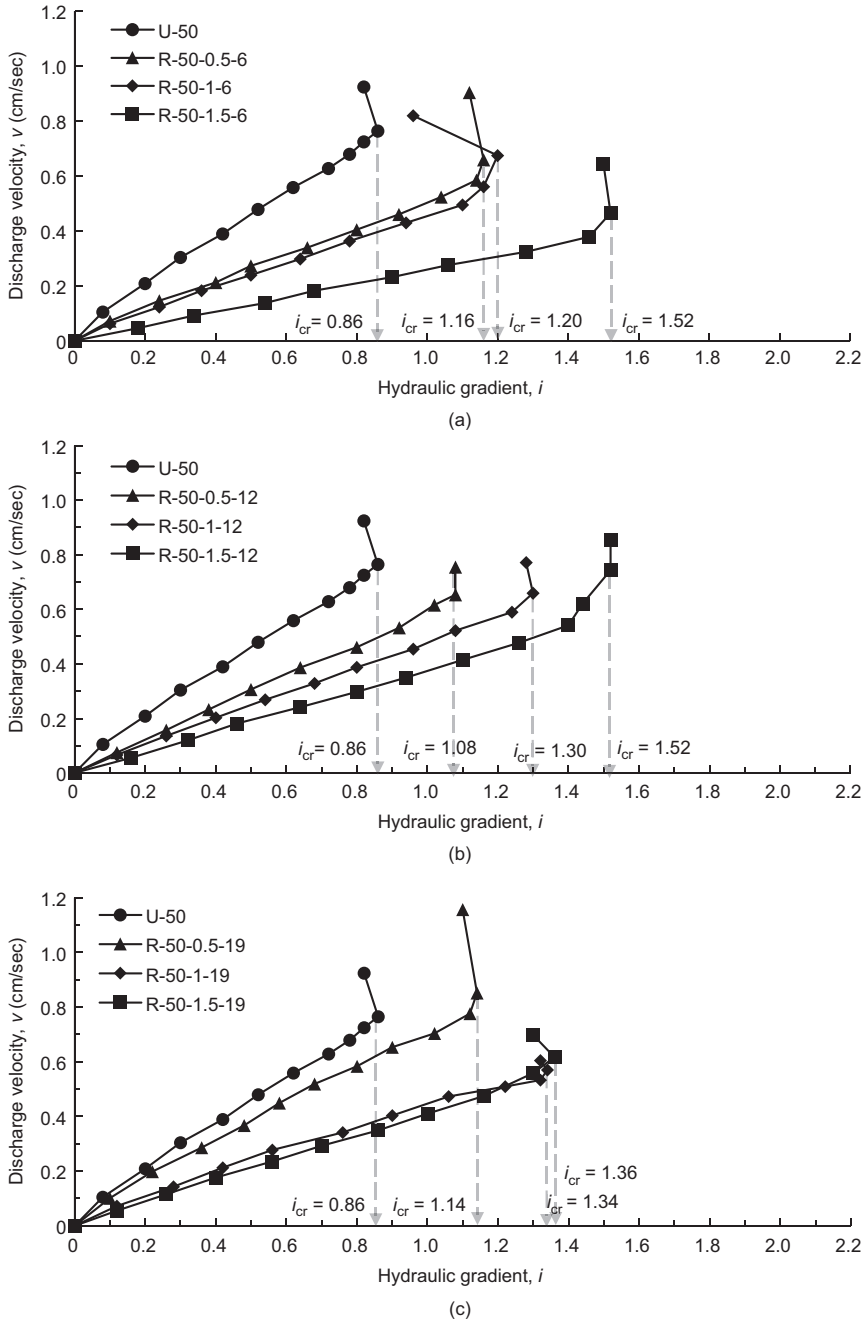

Figure 6. Results for Test Series L: (a) L_f = 6 mm; (b) L_f = 12 mm; (c) L_f = 19 mm

that the pore space of soil in a dense state, which is less abundant and smaller than that of soil in a loose state, could be easily blocked or filled with a given amount of fibre.

Figure 9 shows the influence of fibre length on k and i_{cr} and Table 3 lists the associated k and i_{cr} ratio values. In general, the k values appear to decrease with a decrease in fibre length for specimens at both densities (Figure 9a). That is, compared with long fibre, the short fibre can produce a higher k reduction. For example, for FRS with w_f = 1.5%, the k increases from 2.2×10^{-3} to 3.5×10^{-3} m/s (k ratio increases from 0.27 to 0.43) in Test Series L and from 1.4×10^{-3} to 2.5×10^{-3} m/s (k ratio increases from 0.24 to 0.41) in Test Series D, respectively, as the fibre length increases from 6 to 19 mm. Better performance in short fibre (i.e. producing a low k value) is likely because the total amount of short fibre is greater than that of long fibre at the given fibre content, resulting in short fibre possibly being able to fill more pore space than long fibre can. Finally, the variation of i_{cr} with fibre length does not show a clear trend (Figure 9b), suggesting that the fibre length has only a minor influence on the i_{cr}. In summary, test results suggest that FRS, prepared with high fibre content and short fibre length, and compacted into a dense soil state, has a superior hydraulic performance for the improvement of soil piping resistance and the reduction of seepage velocity.

3.4. Relationship between soil shear strength and critical hydraulic gradient

A series of direct shear tests was performed to establish the relationship between the soil shear strength and the

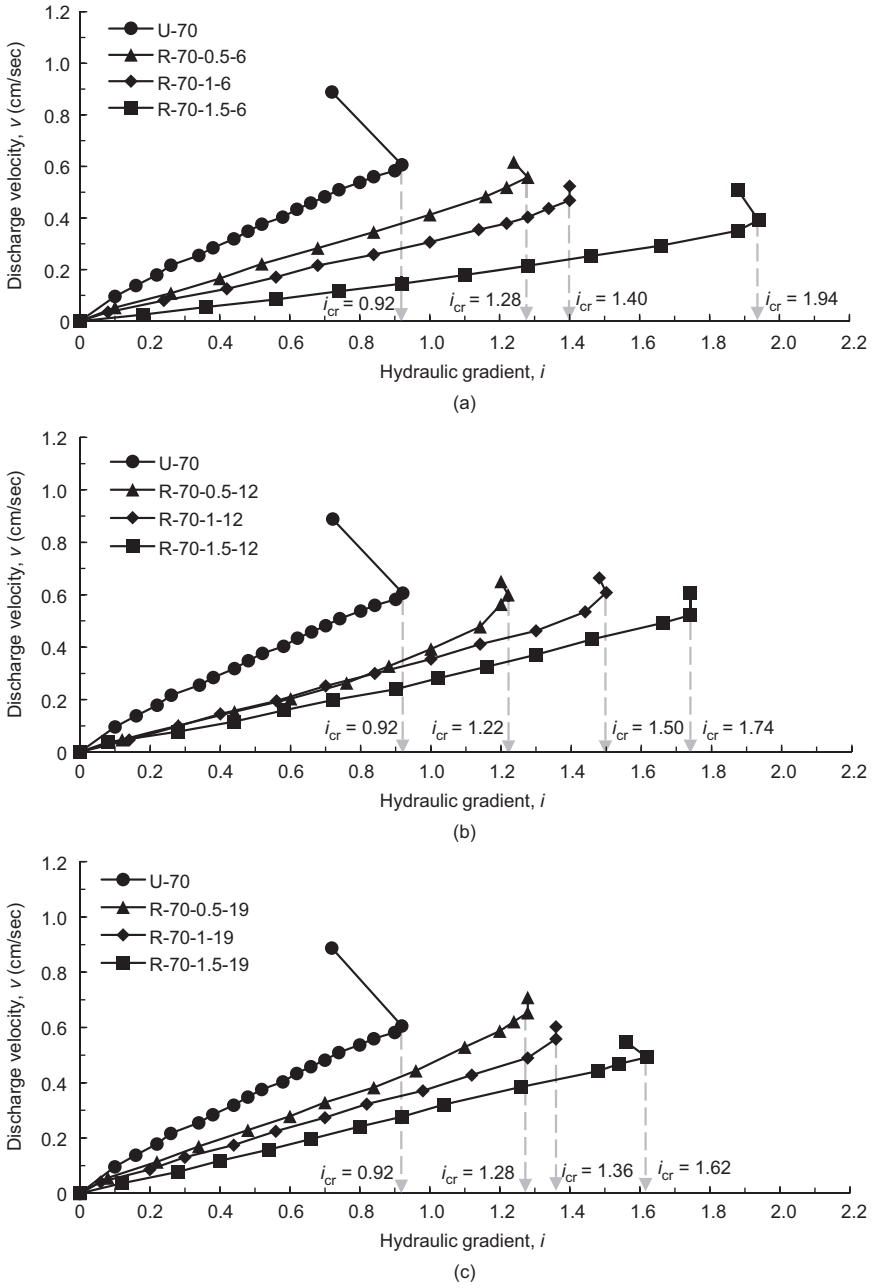

Figure 7. Results for Test Series D: (a) $L_f = 6$ mm; (b) $L_f = 12$ mm; (c) $L_f = 19$ mm

critical hydraulic gradient. The direct shear test was conducted in accordance with ASTM D3080. The specimen size was 6.33 cm in diameter of and 4.66 cm in height, subjected to normal pressures of 100, 200, and 400 kPa, under a shearing rate of 1.5 mm/min. The failure was determined corresponding to the maximum shear stress measured, or the shear stress at the relative displacement of 10 mm for the cases where no definite peak was noticed on the stress-displacement curve. The specimens were prepared in the same manner as the ones used for the seepage tests. The quantity of soil and fibre was calculated according to the expected specimen volume and fibre content. The soil and fibre were carefully mixed and then the sand-fibre mixture was placed in four layers into the shear box. The specimens were also moisturised to avoid soil–fibre segregation.

Figure 10 shows the direct shear test results of the loose and dense specimens prepared with different fibre contents. Specimens with higher fibre content gained higher shear strength, indicating a greater soil–fibre interaction when the number of fibres per volume increased. This observation is consistent with results reported by many other studies on the mechanical behavior of FRS (e.g. Maher and Gray 1990; Michalowski and Zhao 1996; Li and Zornberg 2013).

The peak soil shear strength τ_f for the specimens in the seepage test were determined from the Mohr–Coulomb failure envelopes (Figure 10) using normal pressure in accordance with the overburden pressure at the bottom of specimens (≈4 kPa). After obtaining the peak shear strength of reinforced and unreinforced sand, the relationship between the soil shear strength and critical hydraulic

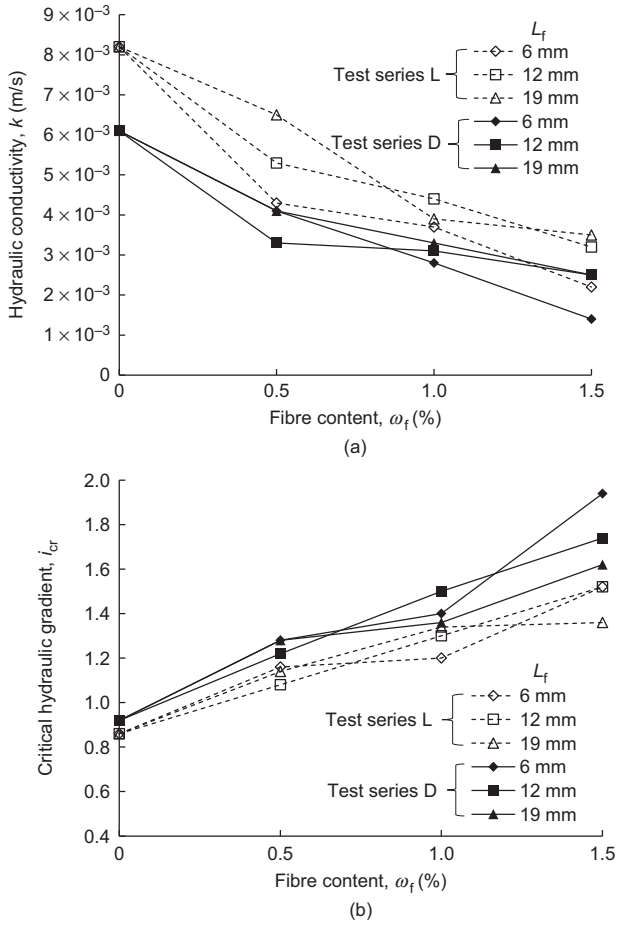

Figure 8. Effect of fibre content on: (a) hydraulic conductivity: (b) critical hydraulic gradient

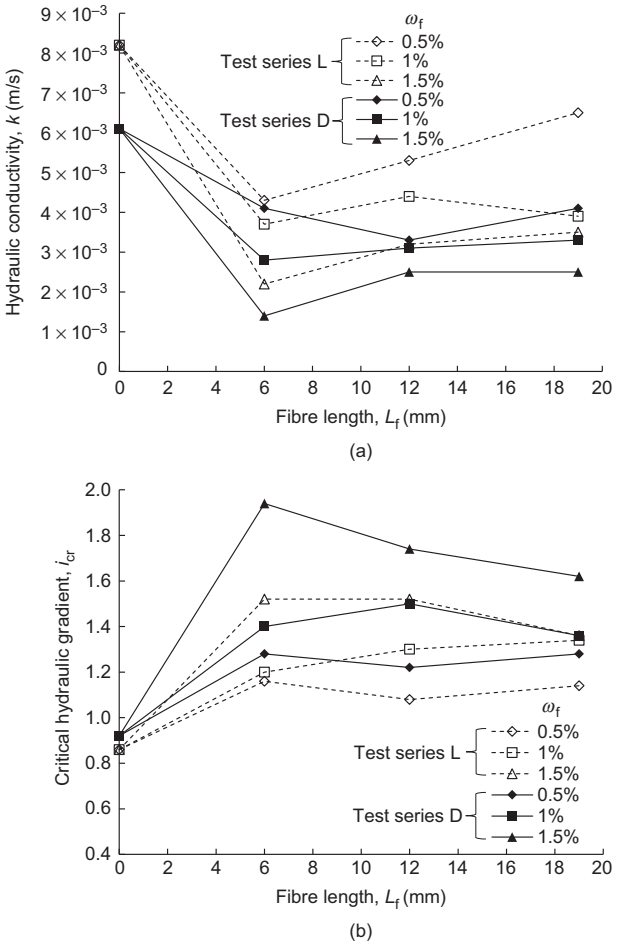

Figure 9. Effect of fibre length on: (a) hydraulic conductivity: (b) critical hydraulic gradient

gradient can be established (Figure 11). As shown in Figure 11, the i_{cr} was strongly correlated with soil τ_f. The data from specimens at different soil densities and fibre parameters fell into a unique linear relationship. This linear relationship demonstrated that the soil shear strength improvement from the fibre inclusion directly contributed to the piping resistance of FRS. This strong correlation between the soil shear strength and critical hydraulic gradient could be also related to the global and isotropic expansion failure mode of FRS, as discussed in Section 3.1. It should be noted that the established relationship cannot be extrapolated because it was established based on the results of the soil tested under low overburden pressures, representing the cases of soils at a shallow depth underneath the surface of geotechnical earth structures. Further study is required to investigate the influence of the overburden pressure on the τ_f and i_{cr} relationship.

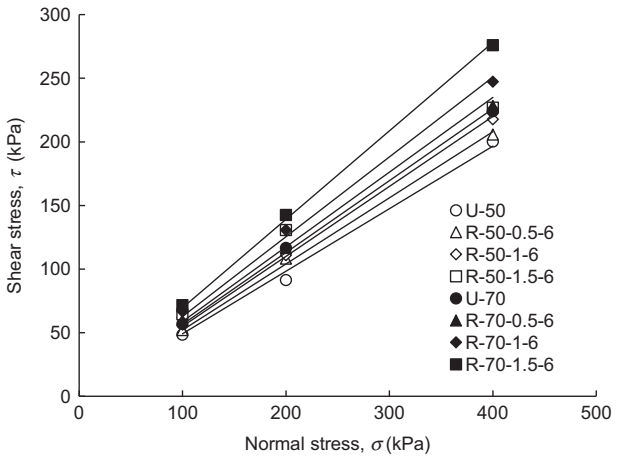

Figure 10. Mohr–Coulomb failure envelopes of loose and dense specimens prepared with different fibre contents

4. DATASET AND COMPARISON

A dataset of seepage tests on FRS was compiled from the literature, including test results reported in Estabragh *et al*. (2014), Das and Viswanadham (2010), Furumoto *et al*. (2002), and Sivakumar Babu and Vasudevan (2008), as well as the test results obtained in this study. The overall variation of hydraulic responses of FRS with fibre content is discussed in this section. Table 4 summarises the soil and fibre parameters and test results from the selected reference. The i_{cr} values in Table 4 were directly adopted from the relevant tables provided in the references. Because these studies mainly focus on the i_{cr} of FRS

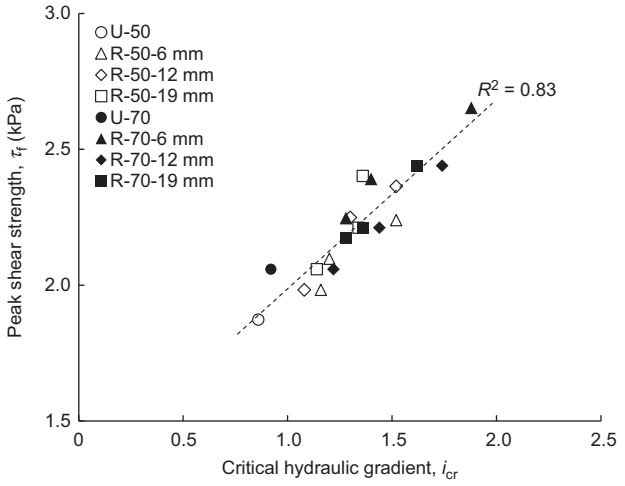

Figure 11. Relationships between critical hydraulic gradient and soil shear strength

rather than the k of FRS, the k values were calculated from the plotted i–v curves according to Darcy's law.

Regarding Table 4, it should be noted that silty sands, consisting of 23% and 20% fine particles, were used in Estabragh *et al*. (2014) and Das and Viswanadham (2010). The fine soils were silt in Estabragh *et al*. (2014) and 10% silt and 10% clay in Das and Viswanadham (2010). In addition, the compiled dataset involves tests with different fibre types, including a natural fibre (i.e. coir) in Sivakumar Babu and Vasudevan (2008), and synthetic fibres (i.e. PE, PET, and PP) in other studies. Das and Viswanadham (2010) experimentally compared the effect of PP and PET fibres on the hydraulic response of FRS and found that soil piping resistance increased by approximately 30–40% for soil reinforced with PP fibre compared with PET FRS. They explained that at a given fibre content, fibre with large specific gravity has a low total volume (or number) of fibres, and hence reduces the benefit of improving soil piping resistance.

Figure 12 shows the overall comparison of the variation of k and i_{cr} ratios with fibre content. In general, the data display a decreasing trend in the k ratio (Figure 12a) and an increasing trend in the i_{cr} ratio (Figure 12b), which agrees well with the experimental results in this study. The large scatter in Figure 12a is because the measured k values of FRS were also influenced essentially by the fibre length and type, as discussed previously. In contrast to Figure 12a, the data of the i_{cr} ratio are less scattered because the measured i_{cr} values were mainly a function of fibre content. Notably, the decreasing trend in the k ratio and the increasing trend in the i_{cr} ratio from Das and Viswanadham (2010) are steeper than those from other studies. Influence from clay content is likely responsible for this difference. As summarised in Table 4, the test soil used by Das and Viswanadham (2010) contains 10% clay. The comparison results in Figure 12 indicate that adding a small amount of clay can significantly improve the efficacy of fibre on the hydraulic performance of FRS. Nevertheless, these findings are based on limited test data. Additional investigations on the hydraulic responses of FRS with a small amount of clay are required to reach a clear conclusion.

5. NUMERICAL EVALUATION

5.1. Case example

A series of transient seepage and slope stability analyses of reinforced and unreinforced embankments subject to flood are described in this section. The combined merits of soil improvement by fibre in both mechanical and hydraulic performance (i.e. increasing soil shear strength and piping resistance) were evaluated numerically. The combined effect on the overall performance of hydraulic structures backfilled with FRS has not been fully investigated. To the best of the authors' knowledge, only one relevant study (Furumoto *et al*. 2002) can be found in the literature. Furumoto *et al*. (2002) conducted 3 m high model tests to investigate the applicability of short FRS layers on river levee structures. They found that short FRS layers increased the stability of levees against rainfall and flood-induced seepage.

Figure 13 shows a hypothetical case example and numerical mesh evaluated in this study. The embankment is 5 m high and 6.5 m wide at the top and has a facing slope of 1H:1V (45°). The effect of concrete facing was not modeled, assuming the worst case scenario by considering that the concrete facing had malfunctioned as a result of damage from previous flood events and had deteriorated with time. A flood history, as illustrated in Figure 13, was applied to the upstream slope boundary; the total flood period is 5 h, in which the water level on the upstream side increased from datum to the maximum water level (3.9 m) over the first 2 h, with the maximum water level maintained for the following hour, and returned to the initial water level over the final 2 h. Two cases, embankments backfilled with unreinforced soil and FRS, were analysed. The numerical results of the hydraulic gradient and the slope factor of safety were examined to evaluate the effect of FRS on improving system piping resistance and stability.

5.2. Numerical analyses

Transient seepage and slope stability analyses were conducted using GeoStudio (SEEP/W and SLOPE/W) software. The embankment model consists of 3602 three-node triangular elements (Figure 13) with a global height of each element of approximately 0.2 m. A head boundary was specified on the upstream slope (0 to 3.9 m), whereas a specified pressure-head condition ($h_p = 0$ m) was assigned to the downstream slope to model a free-draining surface. Zero-flux boundary conditions were set on both the top and bottom sides of the embankment.

Soil, in reality, gradually varies from dry to wet conditions during the transient seepage process (Polemio and Lollino 2011; Stark *et al*. 2017). Hence, the soil was modeled as a 'saturated/unsaturated' material to account for the unsaturated condition of the soil. The soil–water characteristic curve (SWCC) was estimated from the grain

Table 4. Summary of fibre reinforced soil tests in the literature

Reference	Soil					Fibre					Test results		
	Soil type (USCS)	% of fine	d_{50} (mm)	d_{10} (mm)	D_r (%)	Fibre type	G_{sf}	d_f (mm)	L_f (mm)	ω_f (%)	Number of tests	i_{cr}	k (m/s)
Estabragh *et al.* (2014)	Silty sand (SM)	23[a]	0.15	0.05	100[b]	PE, PET	0.91, 1.27	0.28, 0.20	5, 25, 35	0.5, 0.75, 1, 1.25	25	1.55–3.15	1.0×10^{-6}–2.3×10^{-6}
Das and Viswanadham (2010)	Silty sand (SM)	20[c]	0.25	0.001	85	PP, PET	0.91, 1.33	0.03–0.055	25, 50	0.05, 0.1, 0.15	13	1.5–3.5	2.24×10^{-8}–1.02×10^{-6}
Furumoto *et al.* (2002)	Sand (SP)	0.5	N/A	N/A	>50[d]	PET	N/A	0.045	64	0.1, 0.2, 0.4	4	1.86–4.18	8.85×10^{-6}–1.4×10^{-5}
Sivakumar Babu and Vasudevan (2008)	Sand (SP)	0	N/A	N/A	N/A	Coir	1.12	0.25	50	0.5, 1, 1.5	4	0.92–1.47	4.1×10^{-4}–8.7×10^{-4}
This study	Sand (SP)	0	1.12	0.61	50, 70	PP	0.91	0.056	6, 12, 19	0.5, 1, 1.5	20	0.86–1.88	1.4×10^{-3}–8.2×10^{-3}

[a]23% of fines is silt.
[b]Relative compaction $R = 100\%$ (compacted to maximum dry unit weight by standard Proctor compaction). The relative density is estimated using $R = 80 + 0.2D_r$ by Lee and Singh (1971).
[c]In 20% of fines, 10% is silt and 10% is clay.
[d]Relative compaction $R = 90\%$. The relative density is estimated using $R = 80 + 0.2D_r$ by Lee and Singh (1971).

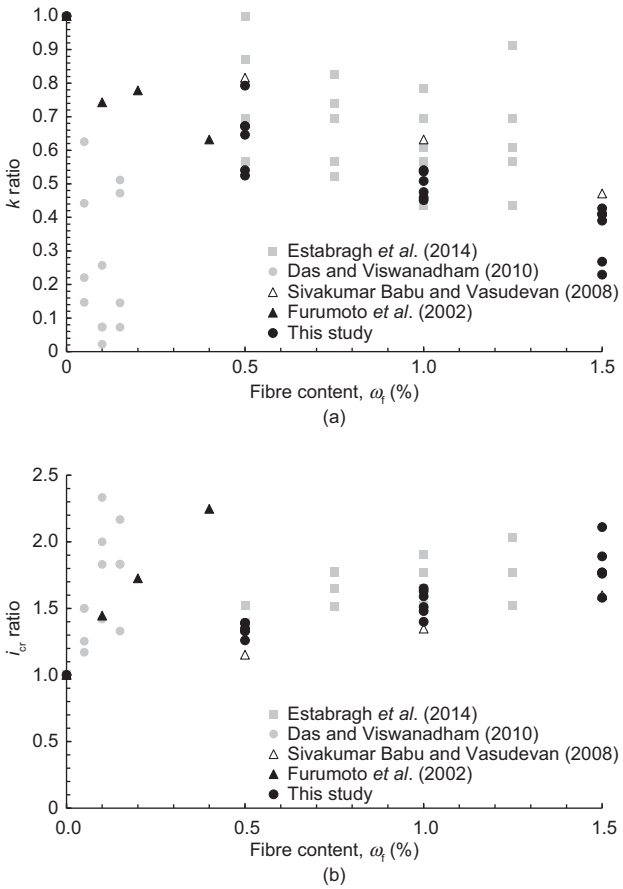

Figure 12. Overall comparison: (a) hydraulic conductivity ratio; (b) critical hydraulic gradient ratio

size distribution (Figure 2) using the modified Kovacs method, as coded in SEEP/W, proposed by Aubertin *et al.* (2003). The van Genuchten–Mualem model (van Genuchten 1980) was used to fit the estimated SWCC and to predict the hydraulic conductivity function (k-function). The determined curve fitting parameters of the SWCC of the soil are $\alpha = 1.14$ kPa, $n = 3.96$, $\theta_s = 31.31\%$, and $\theta_r = 0.97\%$ (where α and n are the SWCC curve fitting parameters; θ_s is the saturated volumetric water content; and θ_r is the residual volumetric water content). Two soils, namely unreinforced sand (U-70) and FRS (R-70-1.5-6), were modeled as backfills. The saturated hydraulic conductivity and friction angle of these two soils, obtained from the experimental tests in this study, were used as input values.

In transient seepage analysis, the flood history was applied to the upstream slope boundary. Each hydraulic head increment was 0.1 m, and the system at each given head increment was solved for numerical convergence. In slope stability analyses, the limit equilibrium calculation was performed using Spencer's method (Spencer 1967), which satisfies all equilibrium conditions. A circular failure surface was assumed in the analysis.

5.3. Results and discussion

The numerical results of the phreatic surface within the embankment, hydraulic gradient near the toe of the

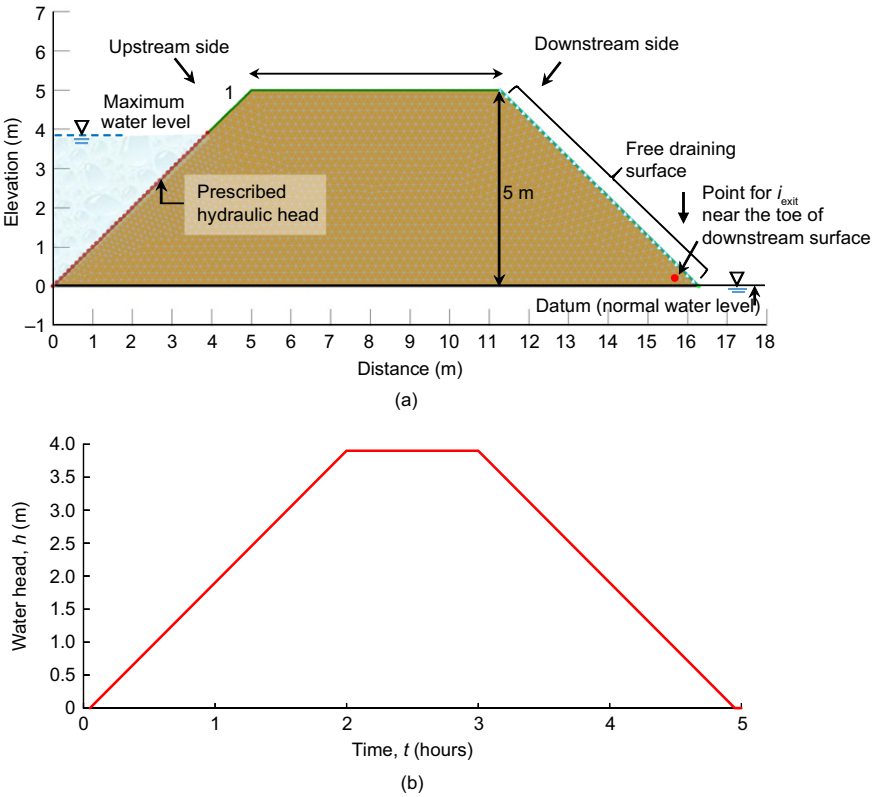

Figure 13. Case example: (a) numerical model and mesh; (b) flood history applied on the upstream slope boundary

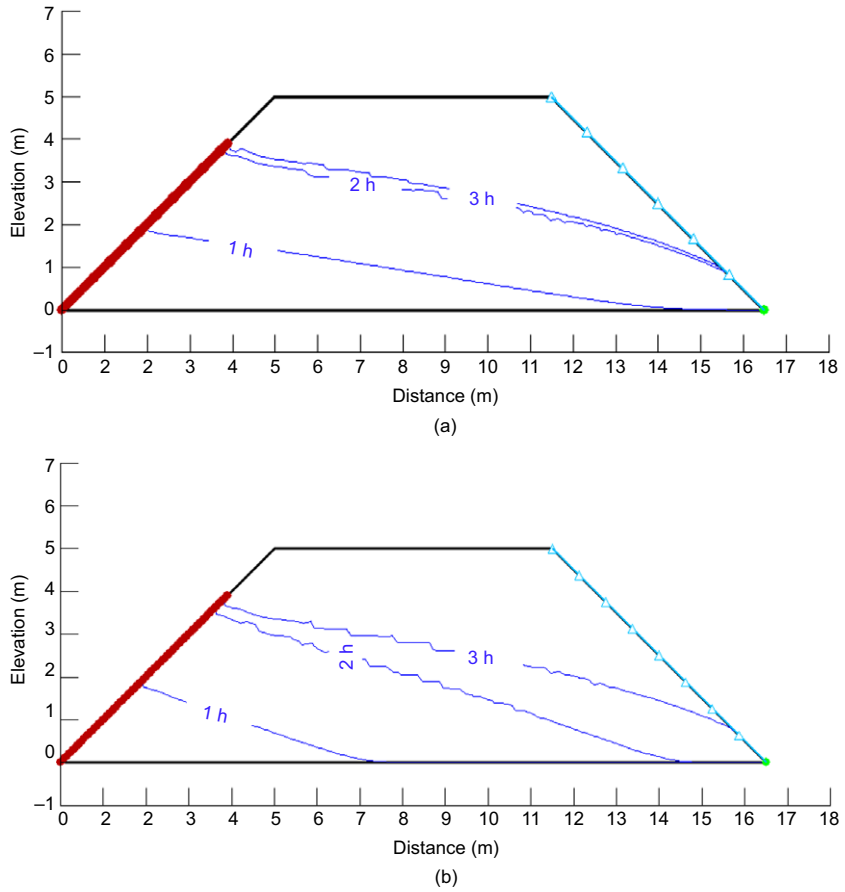

Figure 14. Variation of phreatic surface within embankments at various times: (a) unreinforced embankment (U-70); (b) reinforced embankment (R-70-1.5-6)

downstream surface i_{exit}, and the slope factor of safety of FS at the downstream slope are discussed in this section. Figure 14 depicts the variation of the phreatic surface within the embankments at various times. The phreatic surface within unreinforced embankment (Figure 14a) rose and reached the toe at the downstream side faster than that within the reinforced embankment (Figure 14b). This is because the permeability of the FRS (R-70-1.5-6) is approximately 4 times lower than that of unreinforced soil (U-70). For the unreinforced embankment, the phreatic surface rose to its maximum elevation immediately after the water level on the upstream side reached its maximum level at $t = 2$ h. The phreatic surface within the unreinforced embankment remained nearly the same elevation from $t = 2$–3 h, indicating that the seepage flow had reached steady-state conditions during this period. By contrast, a visible difference in phreatic surface within the reinforced embankment existed between $t = 2$ and 3 h. A comparison of the phreatic surface within the unreinforced and reinforced embankments suggests that the FRS can effectively defer the advance of seepage because of its low permeability.

Figure 15 shows the variation of FS with time at the downstream slope. As the seepage progressed, the FS of the unreinforced embankment decreased soon after the seepage flow reached the downstream slope at $t = 1$ h. The FS of the unreinforced embankment decreased to below FS = 1.0 at $t = 1$–2 h, indicating that slope failure occurred because of the influence of elevated phreatic surface-induced seepage, as shown in Figure 14. The computation of the FS was continued for FS < 1.0 to demonstrate the recovery of the FS after the water level subsided. The FS of the reinforced embankment at $t = 0$ h (initial conditions) was higher than that of the unreinforced embankment because FRS has a higher friction angle than unreinforced soil, as discussed in Section 3.4. As seepage continued, the FS of the reinforced embankment started to decrease after $t = 2$ h. Compared with the timing of the decrease of FS of the unreinforced embankment, the reinforced embankment exhibited greater resistance to the advance of seepage. The FS of the reinforced embankment remained larger than FS = 1.0 during the entire flood event, demonstrating the effectiveness of FRS on improving system stability against seepage.

Figure 16 shows the variation of soil piping potential (SPP) with time near the toe of the downstream slope.

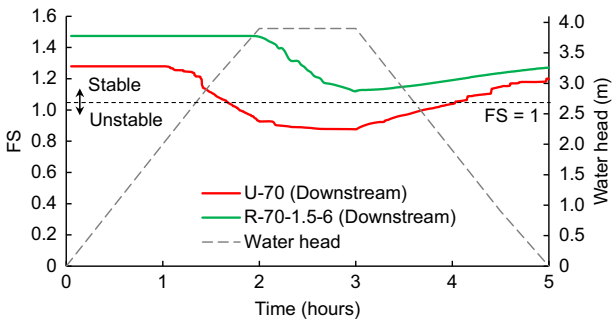

Figure 15. Variation of factor of safety at the downstream slope with time

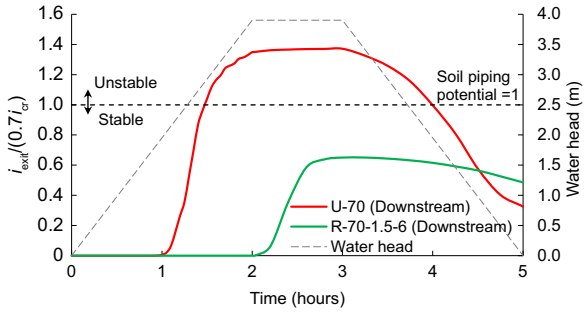

Figure 16. Variation of soil piping potential near the toe of the downstream slope versus time

The SPP is defined as follows:

$$\text{SPP} = \frac{i_{\text{exit}}}{0.7 i_{\text{cr}}} \tag{4}$$

where i_{exit} is the exit hydraulic gradient at the toe of the downstream slope and i_{cr} is the critical hydraulic gradient of soil subject to upward seepage. The values of i_{exit} were obtained from the transient seepage analysis and the values of i_{cr} were obtained from the experimental tests of U-70 and R-70-1.5-6 in this study. Based on the observation of flow vectors within the embankment, the seepage at the toe of the downstream slope almost flowed along a horizontal direction. To account for the effect of horizontal seepage on i_{cr}, a factor of 0.7 was multiplied by i_{cr} in Equation (4), according to the suggestion by Skempton and Brogan (1994), in which the critical hydraulic gradient of soil subject to horizontal seepage is approximately 0.7 times that subject to vertical seepage. The difference in critical hydraulic gradients in different seepage directions results from the influence of gravity acting in the vertical direction (Skempton and Brogan 1994).

Figure 16 shows that when seepage advances to the downstream slope of the unreinforced embankment, the SPP exceeds 1.0 at $t = 1$–2 h, indicating that soil piping and erosion failure could occur. In contrast, the downstream slope of the reinforced embankment remains hydraulically stable (no soil piping or erosion failure occurs) because the calculated SPP is much lower than 1.0 for the entire flood event. The comparison results in Figure 16 demonstrate the effectiveness of FRS on enhancing the soil piping resistance. In summary, numerical studies suggest that the use of FRS as backfill can effectively delay seepage infiltration, reduce soil piping potential, and improve system slope stability against seepage.

6. CONCLUSIONS

In this study, experimental seepage tests were conducted to investigate the hydraulic responses (i.e. piping failure mode, hydraulic conductivity, and critical hydraulic gradient) of FRS subject to seepage. A dataset of seepage tests on FRS was compiled from the literature to assess the overall variation of k and i_{cr} with fibre

content. Numerical simulations of unreinforced and reinforced embankments subjected to flooding were performed. The combined merits of soil improvement using fibre in both mechanical and hydraulic performance were evaluated numerically. Based on the experimental and numerical observations and interpretations of the test results, the following conclusions can be drawn:

(1) Unreinforced specimens had a failure mode associated with a significant soil heave and vigorous soil piping/boiling, whereas the reinforced specimens exhibited an isotropic failure mode (a uniform soil expansion) with several horizontal microcracks developing within the specimen.
(2) Seepage test results revealed that i_{cr} increases and k decreases as the fibre content increases. The experimental results are likely to result from the fibre inclusion providing tensile resistance against soil piping and erosion, and restricting the seepage flow within some pore channels, which were partially blocked by fibres.
(3) Test results suggested that FRS, prepared with high fibre content and short fibre length, and compacted into a dense soil state, has superior hydraulic performance in the improvement of soil piping resistance and reduction of seepage velocity.
(4) A unique linear relationship exists between i_{cr} and τ_f, indicating that soil shear strength improvement from fibre inclusion directly contributed to the piping resistance of FRS. This strong correlation between the soil shear strength and the critical hydraulic gradient is also related to the global and isotropic expansion failure mode of FRS as observed from the experimental tests.
(5) Data compiled from the literature displayed a decreasing trend in the k ratio and an increasing trend in the i_{cr} ratio as the fibre content increased, which agreed well with the experimental results in this study. Trends in the data from Das and Viswanadham (2010) were notably steeper than those from other studies, suggesting that the hydraulic responses of FRS could be significantly affected by clay content.
(6) Numerical results of transient seepage and slope stability analyses on reinforced and unreinforced embankments subject to flooding proved that an embankment backfilled with FRS possesses the combined merits of soil improvement in both mechanical and hydraulic performance. The use of FRS as backfill can effectively delay the advance of seepage, reduce the soil piping potential, and improve system slope stability against seepage.

Based on the comparison of experimental data compiled from the literature, this study found that adding a small amount of clay can significantly improve the hydraulic performance of FRS; however, more data must be collected to reach a clear conclusion. For future studies, the hydraulic responses of FRS with a small amount of clay are advised. In addition, the numerical simulations conducted in this study focused on the performance of an embankment *fully* backfilled with FRS. The effect of FRS *partially* backfilled into an embankment (e.g. placing FRS only in the central area of an embankment, applying FRS for embankment slope covers, or layering FRS horizontally as reinforcing layers at a certain vertical spacing) is a noteworthy topic for further evaluation.

ACKNOWLEDGEMENTS

The financial support for this research was from the Ministry of Science and Technology of Taiwan under grant no. MOST105-2221-E-011-038. The financial support for the second author was provided by the Taiwan Ministry of Education under the grant for 'Aim for the Top-Tier University Project'. These financial supports are gratefully acknowledged.

NOTATION

Basic SI units are given in parentheses.

C_c coefficient of curvature (dimensionless)
C_u uniformity coefficient (dimensionless)
D_r soil relative density (dimensionless)
d_{10} effective particle size (m)
d_{50} mean particle size (m)
d_f average fibre diameter (m)
e target void ratio (dimensionless)
e_{max} maximum void ratio (dimensionless)
e_{min} minimum void ratio (dimensionless)
FS factor of safety (dimensionless)
G_s specific gravity of natural soil (dimensionless)
G_{sf} specific gravity of fibre (dimensionless)
H specimen height (m)
h water level on upstream side of embankment (m)
i hydraulic gradient (dimensionless)
i_{cr} critical hydraulic gradient (dimensionless)
i_{exit} hydraulic gradient at the toe of the downstream slope (dimensionless)
k hydraulic conductivity (m/s)
L distance between the two measuring valves (m)
L_f fibre length (m)
n, α soil–water characteristic curve fitting parameters
SPP soil piping potential (= $i_{exit}/0.7i_{cr}$) (dimensionless)
t time (s)
v discharge velocity (m/s)
W_f dry weight of fibre
W_s dry weight of soil
$\gamma_{d,max}$ maximum dry unit weight of sand (N/m^3)
$\gamma_{d,min}$ minimum dry unit weight of sand (N/m^3)
Δh differential hydraulic head (m)
Δi applied hydraulic head (m)
θ_r residual volumetric water content
θ_s saturated volumetric water content
σ normal stress (Pa)
τ_f peak shear strength (Pa)
ω_f gravimetric fibre content (dimensionless)

REFERENCES

Ahmad, F., Bateni, F. & Azmi, M. (2010). Performance evaluation of silty sand reinforced with fibres. *Geotextiles and Geomembranes*, **28**, No. 1, 93–99.

Anggraini, V., Asadi, A., Huat, B. B. K. & Nahazanan, H. (2015). Effects of coir fibers on tensile and compressive strength of lime treated soft soil. *Measurement*, **59**, 372–381, https://doi.org/10.1016/j.measurement.2014.09.059.

ASTM D2434 *Standard Test Method for Permeability of Granular Soils (Constant Head)*. ASTM International, West Conshohocken, PA, USA.

ASTM D3080 *Standard Test Method for Direct Shear Test of Soils Under Consolidated Drained Conditions*. ASTM International, West Conshohocken, PA, USA.

ASTM D4253 *Standard Test Methods for Maximum Index Density and Unit Weight of Soils Using a Vibratory Table*. ASTM International, West Conshohocken, PA, USA.

ASTM D4254 *Standard Test Methods for Minimum Index Density and Unit Weight of Soils and Calculation of Relative Density*. ASTM International, West Conshohocken, PA, USA.

Aubertin, M., Mbonimpa, M., Bussière, B. & Chapuis, R. P. (2003). A model to predict the water retention curve from basic geotechnical properties. *Canadian Geotechnical Journal*, **40**, No. 6, 1104–1122.

Brandl, H. (2011). Geosynthetics applications for the mitigation of natural disasters and for environmental protection. *Geosynthetics International*, **18**, No. 6, 340–390.

Chou, J. S., Yang, K. H. & Lin, J. Y. (2016). Peak shear strength of discrete fiber-reinforced soils computed by machine learning and metaensemble methods. *Journal of Computing in Civil Engineering, ASCE*.

Collins, R., Zhang, M., Zhang, X., Hulsey, L., Ravens, T. & Van Veldhuizen, R. (2015). Evaluation of geofibers and nontraditional liquid additives on erodible slopes in Interior Alaska. *Geotextiles and Geomembranes*, **43**, No. 5, 412–423.

Consoli, N. C., Montardo, P., Prietto, M. & Pasa, S. (2002). Engineering behavior of a sand reinforced with plastic waste. *Journal of Geotechnical and Geoenvironmental Engineering, ASCE*, **128**, No. 6, 462–472.

Consoli, N., Casagrande, M. & Coop, M. (2005). Effect of fiber reinforcement on the isotropic compression behavior of a sand. *Journal of Geotechnical and Geoenvironmental Engineering, ASCE*, **131**, No. 11, 1434–1436.

Consoli, N., Casagrande, M. & Coop, M. (2007). Performance of a fibre-reinforced sand at large shear strains. *Géotechnique*, **57**, No. 9, 751–756.

Consoli, N., Festugato, L. & Heineck, K. (2009a). Strain-hardening behaviour of fibre-reinforced sand in view of filament geometry. *Geosynthetics International*, **16**, No. 2, 109–115.

Consoli, N. C., Vendruscolo, M. A., Fonini, A. & Rosa, F. D. (2009b). Fiber reinforcement effects on sand considering a wide cementation range. *Geotextiles and Geomembranes*, **27**, No. 3, 196–203.

Danka, J. & Zhang, L. M. (2015). Dike failure mechanisms and breaching parameters. *Journal of Geotechnical and Geoenvironmental Engineering, ASCE*, **141**, No. 9, 04015039.

Das, A. & Viswanadham, B. V. S. (2010). Experiments on the piping behavior of geofiber-reinforced soil. *Geosynthetics International*, **17**, No. 4, 171–182.

Das, A., Jayashree, C.h. & Viswanadham, B. V. S. (2009). Effect of randomly distributed geofibers on the piping behaviour of embankments constructed with fly ash as a fill material. *Geotextiles and Geomembranes*, **27**, No. 5, 341–349.

De Camillis, M., Di Emidio, G., Bezuijen, A. & Verástegui-Flores, R. D. (2016). Hydraulic conductivity and swelling ability of a polymer modified bentonite subjected to wet–dry cycles in seawater. *Geotextiles and Geomembranes*, **44**, No. 5, 739–747.

Diambra, A., Ibrahim, E., Mui Wood, D. & Russell, A. R. (2010). Fiber reinforced sands: experiments and modelling. *Geotextiles and Geomembranes*, **28**, No. 3, 238–250.

Estabragh, A. R., Soltannajad, K. & Javadi, A. A. (2014). Improving piping resistance using randomly distributed fibers. *Geotextiles and Geomembranes*, **42**, No. 1, 15–24.

Estabragh, A. R., Soltanijad, A. & Javadi, A. A. (2016). Models for predicting the seepage velocity and seepage force in a fiber reinforced silty soil. *Computers and Geotechnics*, **75**, 174–181, https://doi.org/10.1016/j.compgeo.2016.02.002.

Fell, R., Wan, C. F., Cyganiewicz, J. & Foster, M. (2003). Time for development of internal erosion and piping in embankment dams. *Journal of Geotechnical and Geoenvironmental Engineering, ASCE*, **129**, No. 4, 307–314.

Foster, M., Fell, R. & Spannagle, M. (2000). The statistics of embankment dam failures and accidents. *Canadian Geotechnical Journal*, **37**, No. 5, 1000–1024.

Furumoto, K., Miki, H., Tsuneoka, N. & Obata, T. (2002). Model test on the piping resistance of short fiber reinforced soil and its application to river levee. *Proceedings of the 7th International Conference on Geosynthetics*, Nice, France, pp. 1241–1244.

Garner, S. J. & Fannin, R. J. (2010). Understanding internal erosion: a decade of research following a sinkhole event. *International Journal on Hydropower and Dams*, **17**, No. 3, 93–98.

Gray, D. & Al-Refeai, T. (1986). Behavior of fabric-versus fiber-reinforced sand. *Journal of Geotechnical Engineering, ASCE*, **112**, No. 8, 804–820.

Gray, D. & Ohashi, H. (1983). Mechanics of fiber reinforcement in sand. *Journal of Geotechnical Engineering, ASCE*, **109**, No. 3, 335–353.

Hagerty, D. J. (1991a). Piping/sapping erosion. I: basic considerations. *Journal of Hydraulic Engineering, ASCE*, **117**, No. 8, 991–1008.

Hagerty, D. J. (1991b). Piping/sapping erosion. II: identification-diagnosis. *Journal of Hydraulic Engineering, ASCE*, **117**, No. 8, 1009–1025.

Hejazi, S. M., Sheikhzadeh, M., Abtahi, S. M. & Zadhoush, A. (2012). A simple review of soil reinforcement by using natural and synthetic fibers. *Construction and Building Materials*, **30**, 100–116, https://doi.org/10.1016/j.conbuildmat.2011.11.045.

Jamshidi, R., Towhata, I., Ghiassian, H. & Tabarsa, R. (2010). Experimental evaluation of dynamic deformation characteristics of sheet pile retaining walls with fiber reinforced backfill. *Soil Dynamics and Earthquake Engineering*, **30**, No. 6, 438–446.

Khattak, M. J. & Alrashidi, M. (2006). Durability and mechanistic characteristics of fiber reinforced soil–cement mixtures. *International Journal of Pavement Engineering*, **7**, No. 1, 53–62.

Lee, K. L. & Singh, A. (1971). Relative density and relative compaction. *Journal of the Soil Mechanics and Foundations Division, ASCE*, **97**, No. 7, 1049–1052.

Li, C. & Zornberg, J. (2013). Mobilization of reinforcement forces in fiber-reinforced soil. *Journal of Geotechnical and Geoenvironmental Engineering, ASCE*, **139**, No. 1, 107–115.

Li, J., Tang, C., Wang, D., Pei, X. & Shi, B. (2014). Effect of discrete fibre reinforcement on soil tensile strength. *Journal of Rock Mechanics and Geotechnical Engineering*, **6**, No. 2, 133–137.

Liu, J., Wang, G., Kamai, T., Zhang, F., Yang, J. & Shi, B. (2011). Static liquefaction behavior of saturated fiber-reinforced sand in undrained ring-shear tests. *Geotextiles and Geomembranes*, **29**, No. 5, 462–471.

Maher, M. H. & Gray, D. H. (1990). Static response of sands reinforced with randomly distributed fibers. *Journal of Geotechnical Engineering, ASCE*, **116**, No. 11, 1661–1677.

Marin, C., Gomez, R. & Petric, J. (2010). Clay-based composite stabilized with natural polymer and fiber. *Construction and Building Materials*, **24**, No. 8, 1462–1468.

Michalowski, R. & Čermák, J. (2003). Triaxial compression of sand reinforced with fibers. *Journal of Geotechnical and Geoenvironmental Engineering, ASCE*, **129**, No. 2, 125–136.

Michalowski, R. & Zhao, A. (1996). Failure of fiber-reinforced granular soils. *Journal of Geotechnical Engineering, ASCE*, **122**, No. 3, 226–234.

Najjar, S., Sadek, S. & Alcovero, A. (2013). Quantification of model uncertainty in shear strength predictions for fiber-reinforced sand. *Journal of Geotechnical and Geoenvironmental Engineering, ASCE*, **139**, No. 1, 116–133.

Nichols, R. J., Sparks, R. S. J. & Wilson, C. J. N. (1994). Experimental studies of the fluidization of layered sediments and the formation of fluid escape structures. *Sedimentology*, **41**, No. 2, 233–253.

Parekh, M., Kanning, W., Bocovich, C., Mooney, M. A. & Koelewijn, A. R. (2016). Backward erosion monitored by spatial-temporal

pore pressure changes during field experiments. *Journal of Geotechnical and Geoenvironmental Engineering, ASCE*, **142**, No. 10, https://doi.org/10.1061/(ASCE)GT.1943-5606.0001528.

Peng, M. & Zhang, L. M. (2012). Breaching parameters of landslide dams. *Landslides*, **9**, No. 1, 13–31.

Pino, L. F. M. & Baudet, B. A. (2015). The effect of the particle size distribution on the mechanics of fibre-reinforced sands under one-dimensional compression. *Geotextiles and Geomembranes*, **43**, No. 3, 250–258.

Polemio, M. & Lollino, P. (2011). Failure of infrastructure embankments induced by flooding and seepage: a neglected source of hazard. *Natural Hazards and Earth System Sciences*, **11**, No. 12, 3383–3396.

Ranjan, G., Vasan, R. M. & Charan, H. D. (1994). Behaviour of plastic-fiber-reinforced sand. *Geotextiles and Geomembranes*, **13**, No. 8, 555–565.

Rice, J. D. & Duncan, J. M. (2010). Findings of case histories on the long-term performance of seepage barriers in dams. *Journal of Geotechnical and Geoenvironmental Engineering, ASCE*, **136**, No. 1, 2–15.

Rice, J. D., Duncan, J. M. & Davidson, R. R. (2007). Identification of failure mechanisms associated with seepage barriers in dams. *Embankment, Dams, and Slopes, ASCE*, 1–11, https://doi.org/10.1061/40905(224)2.

Richards, K. S. & Reddy, K. R. (2007). Critical appraisal of piping phenomena in earth dams. *Bulletin of Engineering Geology and Environment*, **66**, No. 4, 381–402.

Sadek, S., Najjar, S. & Freiha, F. (2010). Shear strength of fiber-reinforced sands. *Journal of Geotechnical and Geoenvironmental Engineering, ASCE*, **136**, No. 3, 490–499.

Santoni, R., Tingle, J. & Webster, S. (2001). Engineering properties of sand-fiber mixtures for road construction. *Journal of Geotechnical and Geoenvironmental Engineering, ASCE*, **127**, No. 3, 258–268.

Shao, W., Cetin, B., Li, Y., Li, J. & Li, L. (2014). Experimental investigation of mechanical properties of sands reinforced with discrete randomly distributed fiber. *Geotechnical and Geological Engineering*, **32**, No. 4, 901–910.

Sivakumar Babu, G. L. & Vasudevan, A. K. (2008). Seepage velocity and piping resistance of coir fiber mixed soils. *Journal of Irrigation and Drainage Engineering, ASCE*, **134**, No. 5, 668–680.

Sivakumar Babu, G. L., Vasudevan, A. K. & Haldar, S. (2008). Numerical simulation of fiber-reinforced sand behavior. *Geotextiles and Geomembranes*, **26**, No. 2, 181–188.

Skempton, A. W. & Brogan, J. M. (1994). Experiments on piping in sandy gravel. *Géotechnique*, **44**, No. 3, 449–460.

Spencer, E. (1967). A method of analysis of the stability of embankments assuming parallel inter-slice forces. *Geotechnique*, **24**, No. 4, 661–665.

Stark, T., Jafari, N., Zhindon, J. & Baghdady, A. (2017). Unsaturated and transient seepage analysis of San Luis dam. *Journal of Geotechnical and Geoenvironmental Engineering, ASCE*, **143**, No. 2, https://doi.org/10.1061/(ASCE)GT.1943-5606.0001602.

Van Genuchten, M. T.h. (1980). A closed-form equation for predicting the hydraulic conductivity of unsaturated soils. *Soil Science Society of America Journal*, **44**, No. 5, 892–898.

Xu, Y. & Zhang, L. M. (2009). Breaching parameters of earth and rock fill dams. *Journal of Geotechnical and Geoenvironmental Engineering, ASCE*, **135**, No. 12, 1957–1970.

Yetimoglu, T. & Salbas, O. (2003). A study on shear strength of sands reinforced with randomly distributed discrete fibers. *Geotextiles and Geomembranes*, **21**, No. 2, 103–110.

Yetimoglu, T., Inanir, M. & Inanir, O. E. (2005). A study on bearing capacity of randomly distributed fiber reinforced sand fills overlying soft clay. *Geotextiles and Geomembranes*, **23**, No. 2, 174–183.

Yilmaz, Y. (2009). Experimental investigation of the strength properties of sand–clay mixtures reinforced with randomly distributed discrete polypropylene fibers. *Geosynthetics International*, **16**, No. 5, 354–363.

Zhang, L. M., Xu, Y. & Jia, J. S. (2009). Analysis of earth dam failures: a database approach. *Georisk*, **3**, No. 3, 184–189.

Zornberg, J. (2002). Discrete framework for limit equilibrium analysis of fibre-reinforced soil. *Géotechnique*, **52**, No. 8, 59.

The Editor welcomes discussion on all papers published in Geosynthetics International. Please email your contribution to discussion@geosynthetics-international.com